

A&A manuscript no.

(will be inserted by hand later)

Your thesaurus codes are:

3(11.05.2;11.06.2;11.12.2;11.16.1;11.19.7)

ASTRONOMY  
AND  
ASTROPHYSICS  
29.8.2019

# Galaxy evolution at low redshift? – I. Optical counts<sup>\*</sup>

E. Bertin<sup>1,2</sup> and M. Dennefeld<sup>1,3</sup>

<sup>1</sup> Institut d’Astrophysique de Paris, 98bis Boulevard Arago, F-75014 Paris, France

<sup>2</sup> European Southern Observatory, Casilla 19001, Santiago 19, Chile

<sup>3</sup> Université Pierre & Marie Curie, 4, place Jussieu, F-75005 Paris, France

Received 22 December 1995; accepted 2 February 1996

**Abstract.** We present bright galaxy number counts in the blue ( $16 < B_J < 21$ ) and red ( $15 < R < 19.5$ ) passbands, performed over 145 sq. degrees, both in the northern and southern galactic hemispheres. The work was conducted on Schmidt plates digitized with the MAMA machine, and individually calibrated using an adequate number of CCD sequences. We find a relatively large density of bright galaxies implying a “high” normalization of the local luminosity function. Our counts and colour distributions exhibit no large departure from what standard no-evolution models predict to magnitudes  $B_J < 21$ , removing the need for evolution of the non-dwarf galaxy population in the optical, out to  $z \approx 0.2$ . This result disagrees with that of Maddox et al. (1990) on the APM catalog. We show that the APM and similar catalogs may be affected by a systematic magnitude scale error which would explain this discrepancy.

**Key words:** galaxies: evolution – galaxies: fundamental parameters – galaxies: luminosity function – galaxies: photometry – galaxies: statistics

## 1. Introduction

Since Hubble (1926), galaxy number counts have been widely used as a statistical tool for probing the distant universe, with the hope of constraining both its geometry and the evolution of its content. Modern, high efficiency instruments and detectors reach impressive magnitude limits in the optical:  $B_J \approx 28$  (Tyson 1988, Metcalfe et al. 1995a,

Smail et al. 1995), although on a limited area. Galaxy counts done at brighter magnitudes ( $B_J < 21$ ) are equally useful; their interpretation is much less model-dependant because of the smaller lookback-times and weaker cosmological effects. They thus constitute the link between models and deeper counts by providing a normalisation of both space densities and colours at low redshift.

The problem with bright galaxy counts is that they obviously require substantial solid angles to be surveyed in order to provide statistically significant samples. Until very recently, such areas could only be surveyed in a reasonable time using photographic Schmidt plates. Since the mid-eighties, fast microdensitometers coupled with image analysis computer programs have been employed to produce automatically highly complete catalogs from large areas of the high galactic latitude sky like the COSMOS (Heydon-Dumbleton et al. 1989), the MRSP (Seitter 1988), or the APM (Maddox et al. 1990b) galaxy surveys.

The main difficulty when dealing with photographic material concerns flux measurements. Many scientific issues typically require the systematic errors to be kept  $\lesssim 0.1$  mag.. This is quite a difficult task to achieve on large scales, and can be reached only if a large number of *galaxy* standards per Schmidt plate, over the whole magnitude range of the counts, are observed to calibrate the data (Metcalfe et al. 1995b). Having such a high density of photometric standards is practically not possible with very large Schmidt plate surveys, because of the huge observing time it would require. The catalogs extracted from these surveys are therefore likely to be hampered by systematic errors in their photometry, rather than by limited statistics.

In this paper we re-examine galaxy number counts in the blue and red photographic passbands over the magnitude range  $16 < B_J < 21$  and  $15 < R_F < 19.5$ . Our surveyed area is modest (140 sq. deg.), but has been carefully calibrated using a fair density of CCD standards ( $\approx 700$ , half of them being galaxies), as an attempt to keep photometric systematic errors  $\lesssim 0.1$  mag. *over the whole magnitude domain* of the survey. The procedure is described

---

Send offprint requests to: E. Bertin (bertin@iap.fr)

<sup>\*</sup> Based in part on observations made at the CERGA Schmidt Telescope (Observatoire de la côte d’Azur, France), at Observatoire de Haute-Provence (France) and at the European Southern Observatory (La Silla, Chile). ESO red survey, SERC blue survey and CERGA plates were digitized with MAMA (Machine Automatique à Mesurer pour l’Astronomie) which is developed and operated by INSU/CNRS.

in detail in §3, as well as the general data processing. The galaxy number counts are derived and compared to previous studies in §4. Model predictions about number counts and galaxy colour distributions are tested in §5. We finally discuss the implications of our results in §6.

## 2. The data

Our optical catalog was originally built as part of a program of identification of faint IRAS sources on Schmidt plates (Bertin et al. , in preparation) near both ecliptic poles. The 7 selected fields are characterized by a very low infrared cirrus emission, which ensures that the interstellar extinction is negligible in the visible. Their coordinates are given in Table 1. To each field corresponds one plate in the blue photographic passband, and one in the red. Northern plates were taken in France at the CERGA 0.9m Schmidt telescope, while southern ones are copies from the ESO and SERC surveys.

## 3. Data processing

### 3.1. Digitization

The 14 plates were scanned in density mode, with the MAMA microdensitometer, using a  $10\ \mu\text{m}$  step ( $0.65''$ ). The MAMA is able to scan a full plate in a few hours, and provides images with a usable dynamic range quite large compared to similar machines like COSMOS or APM: more than 3 in density (a description of the microdensitometer and its performances can be found in Berger et al. 1991). Because of limitations in acquisition and storage capabilities with the MAMA at that time, the image data were acquired as  $12' \times 12'$  frames, and recombined as  $18' \times 18'$  images, with an overlap of  $6'$  (which therefore defines the maximum size allowed for objects to be reliably measured).

To insure a maximum reliability of the catalog, only the central “clean”  $4.5^\circ \times 4.5^\circ$  of each field were kept for analysis (ESO and CERGA plates cover only slightly more than  $5^\circ \times 5^\circ$  in total, and full coverage was not needed here). The exact areas retained for the final catalogs are reported in Table 1.

### 3.2. Astrometry

The standard MAMA procedure was adopted to calibrate the plates astrometrically (see Berger et al. 1991). Between 150 and 300 suitable astrometric standards (PPM catalog, Röser & Bastian 1991) can be found per plate. A third order fit on projected coordinates leads to a mean residual of  $\approx 0.2''$ , similar to the value obtained when comparing bright object positions between the two passbands. However, this figure degrades noticeably ( $\approx 1''$ ) at the extreme borders of some plates. We had to adjust ESO plates 200 and 249 to their blue counterparts SERC 200

and 249 using a neural network mapping<sup>1</sup> on bright stars to secure blue/red object matching.

### 3.3. Detection

A dedicated version of the SExtractor software (Bertin & Arnouts 1996, hereafter BA96) was used in PHOTO mode for source extraction. The standard 2 pixels ( $1.3''$ ) FWHM SExtractor’s convolution mask was applied in order to improve the detectability of low surface brightnesses<sup>2</sup>. Although emulsion noise becomes strongly correlated on small scales (especially on copies), this technique enables one to lower the detection threshold to a secure  $1.5\sigma$  of the sky background fluctuations, corresponding to mean surface brightnesses  $\mu_{B_J} = 24.9\ \text{mag.arcsec}^{-2}$  (CERGA blue plates),  $\mu_{R_F} = 22.8\ \text{mag.arcsec}^{-2}$  (CERGA red plates),  $\mu_{B_J} = 25.9\ \text{mag.arcsec}^{-2}$  (SERC blue plates) and  $\mu_{R_F} = 23.8\ \text{mag.arcsec}^{-2}$  (ESO red plates).

The deblending capabilities of SExtractor give no limitation to the size of objects which can be extracted; spiral arms and other peripheral substructures of bright galaxies are not “separated” from the central region. Therefore the catalog is expected to be complete for all objects smaller than the overlap between subframes:  $6'$  (corresponding here to  $B_J \approx 12$ ).

### 3.4. Star/galaxy separation

Star-galaxy separation was performed with a dedicated neural network (Bertin 1994) trained on a sample made of bright objects classified by eye, and fainter ones from the CCD photometric fields (§3.5.3). The latter were classified automatically using SExtractor’s tunable neural network classifier (see BA96). Briefly, each detected object is translated into a pattern vector containing basic information about its profile (7 isophotal areas plus the peak density). This combination of parameters, added to the ability of neural networks to deal with complex distributions in multidimensional space, leads to a very robust star/galaxy classifier. In particular, objects affected by optical distortions (in the corner of the plates) or merging (we chose to classify undebled pairs as “stars” if and only if the brightest component is a star) are properly handled. Unfortunately, as we will see, such a set of parameters is not well fitted to the classification of very bright stars and galaxies, which show similar profiles.

A minimum of 500 sample patterns is necessary for the neural network to achieve performances close to its asymptotic values (Bertin 1996); we used  $\approx 800$  per field.

<sup>1</sup> some other examples of using neural networks as an interpolation tool in multidimensional analysis can be found in Serra-Ricart et al. 1995 or Bertin 1996.

<sup>2</sup> In SExtractor, convolution is only applied to the template frame on which objects are detected, not to the image itself; subsequent measurements are unaffected by this operation.

**Table 1.** Schmidt fields

Field	$\alpha$ (2000.0)		$\delta$ (2000.0)		Area* sq. degrees	Plates	
	h	m	°	'		“blue”	“red”
3 <sup>h</sup> -45°	03	46	-44	40	21.57	SERC 249J	ESO 249F
3 <sup>h</sup> -50°	03	32	-49	40	21.89	SERC 200J	ESO 200F
4 <sup>h</sup> -45°	04	13	-44	40	20.74	SERC 250J	ESO 250F
4 <sup>h</sup> -50°	04	01	-49	40	20.38	SERC 201J	ESO 201F
9 <sup>h</sup> +78°	09	22	+78	00	20.38	CERGA 2970J	CERGA 3048F
15 <sup>h</sup> +50°	15	36	+50	00	20.22	CERGA 3074J	CERGA 3063F
16 <sup>h</sup> +42°	16	31	+42	17	20.29	CERGA 3078J	CERGA 3084F

\* used in the final catalog.

Extensive visual checks and colour histograms show that stellar contamination among catalogued galaxies due to misclassifications is less than 4% for  $14 < B_J < 19.5$ , rising to 10% at  $B_J \approx 20$  (CERGA plates) and  $B_J \approx 21$  (UKST plates).  $B_J = 20$  and  $B_J = 21$  therefore define the upper magnitude limits for the northern and southern sets of plates, respectively. The estimated loss of galaxies due to misclassifications is similar to stellar contamination at faint magnitudes. We can rely on statistics from the identifications of optically bright IRAS galaxies (Bertin et al. 1996), which contain less than 10% of objects classified as “stars” for  $B_J > 16$ . As a high fraction of IRAS galaxies turn out to be rather compact and difficult to separate from point-sources on photographic images (Sutherland et al. 1991), this gives us an upper limit of the loss we might expect at these magnitudes. It is more difficult to estimate it precisely at the bright end of our counts ( $B_J < 16$ ), because stars outnumber galaxies by a factor  $> 50$ . We examined 600 detections with  $B_J \approx 15.5$ , classified as stars, and found indeed that 4 of them were galaxies. There seems therefore to be some loss of galaxies at the bright end of our catalog, and counts below  $B_J = 16$  (or  $R_F = 14.5$ ) should only be considered as lower limits.

### 3.5. Photometry

#### 3.5.1. Estimation of magnitudes

The way SExtractor estimates “total” magnitudes on CCD images is described in details in BA96. In the “PHOTO” mode, the program applies a density-to-intensity transformation (see §3.5.2) before summing pixel fluxes. Briefly, for each object, two kinds of magnitudes are computed. The first one is an improvement of Kron’s (1980) method: it measures the flux integrated in an elliptical aperture whose size and shape are function of the object’s profile. The second one is isophotal, and corrects for the fraction of flux lost in the wings (assuming a gaussian profile) as in the APM survey (Maddox et al. 1990c). As this second method is more subject to biases than the first one, we take the aperture magnitude as an estimate of “total” magnitude, unless it is suspected to be contaminated by the presence of neighbours by more than 0.1 mag; in which

case we rely on corrected isophotal magnitude. Such a situation occurs in less than 20% of the cases in our images; SExtractor’s total magnitude is thus essentially an aperture magnitude.

The behaviour of SExtractor’s magnitudes on simulated Schmidt plate images is shown in Fig. 1. The predicted fraction of flux measured for galaxies is remarkably constant with magnitude, even beyond the completeness limit. As can be seen, the mean offset one needs to apply to SExtractor’s magnitude to get an estimate of “total magnitude” is  $\approx -0.06$  mag.

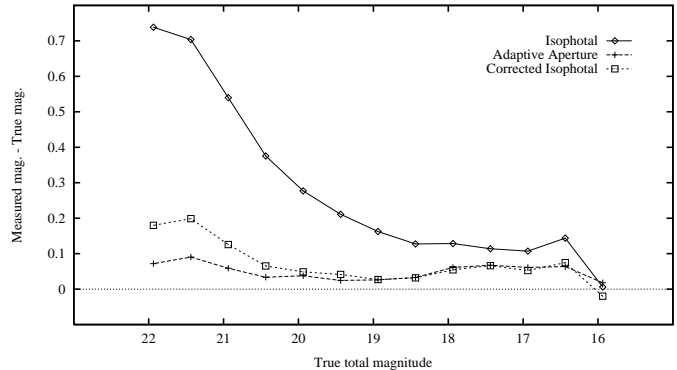


**Fig. 1.** Prediction of the mean flux lost (expressed in magnitude) by SExtractor’s isophotal, corrected isophotal and adaptive aperture magnitudes, as a function of the “true” total magnitude. These estimates are from simulated Schmidt plates images, generated as described in BA96. The simulations are done in the blue photographic passband; they assume a logarithmic response of the emulsion and image parameters typical of CERGA Schmidt plates, with a seeing FWHM of  $2''$ . The apparent drop seen at  $B_J = 16$  is an artefact due to poor statistics.

#### 3.5.2. Linearization of the photographic response

In PHOTO mode, SExtractor transforms densities  $D$  to intensities  $I$  during image analysis assuming a logarithmic response of the emulsion in the “linear part”:

$$I = I_0 \cdot 10^{\frac{D}{\gamma}} \quad (1)$$

where  $\gamma$  defines the contrast of the emulsion (as measured with MAMA), and  $I_0$  is the intensity zero-point. Both parameters were adjusted for each plate by minimizing the  $\chi^2$  on “total magnitudes” estimated by SExtractor for a set of CCD standard galaxies. For all plates but one we found  $2 < \gamma < 3$ . Differential desensitization and telescope vignetting were compensated for by subtracting the local background density from  $D$  before applying the calibration law (Eq. 1). This correction is perfectly valid here as no interstellar emission is expected in these fields, and reduces large-scale sensitivity variations to  $\lesssim 0.1$  mag (Bertin 1996).

Finally, for galaxies, a linear least-square fit was applied separately to the magnitude scale in each field to correct for residual differences of  $\approx \pm 3\%$  in the slope of the relation between photographic and CCD magnitudes. Bright stellar images are affected by a mix of photographic saturation, complex chemical proximity effects and, above all, light diffusion inside the emulsion during the scanning process. Stars thus need a specific calibration which was carried out using polynomial and neural network fits between their photographic and CCD magnitudes.

Eq. (1) provides a good fit to photographic calibration curves of sky-limited exposures measured with MAMA (Moreau 1992, Bertin 1996), although it does not take into account possible saturation effects. Thanks to the fairly large dynamic range of MAMA, saturation affects our galaxy magnitudes to a lesser extent than e.g. APM or COSMOS scans. Nevertheless, southern *copy* plate images unambiguously show some signs of saturation on cores of galaxies with  $B_J \lesssim 17$ . We therefore expect that both systematic and random errors increase significantly towards brighter magnitudes on these plates (see Metcalfe et al. 1995b for a discussion about the consequences of saturation on galaxy photometry).

### 3.5.3. CCD calibration and colour equations

A total of 30 photometric CCD fields ( $\approx 4$  per Schmidt field, centered on groups of bright galaxies) were taken essentially at the OHP 1.2m and the ESO 2.2 and 3.6 meter telescopes, and matched to Cousins B and R magnitudes. SExtractor was also used at all stages of the CCD data reduction, leading to “total magnitudes” for about 1000 objects. As northern and southern plate sets have been taken with slightly different filter combinations, we naturally expect differences in their related colour equations. However we need to keep the survey as close as possible to a uniform (and as standard as possible) passband system. Following Blair & Gilmore (1982), we define here the blue passband  $B_J$  as

$$B_J \equiv B - 0.28(B - V) \approx B - 0.19(B - R) \quad (2)$$

which is the transformation also adopted in the APM survey. The  $R_F$  band is defined as

$$R_F \equiv R \quad (3)$$

B, V and R are in the Cousins system<sup>3</sup>. Figure 2 shows the distribution of the residuals as a function of the  $B_J - R$  CCD colour index for each of the 4 types of plates. Although they are moderate, one can see systematic colour effects. The “best fit” colour coefficients are reported in Table 3.5.3. For CERGA blue plates the results are in good agreement with the estimates of Majewski (1992), who finds  $B_{\text{IIIaJ+GG385}} = B - 0.23(B - V)$ . We find a stronger colour coefficient for the SERC passband than the one traditionally used at the APM ( $B_{\text{IIIaJ+GG395}} = B - 0.28(B - V)$ ), and conflicting even more with the COSMOS ( $B_{\text{IIIaJ+GG395}} = B - 0.23(B - V)$ )<sup>4</sup>. However our estimate is in remarkable agreement with the recent and accurate measurements by Metcalfe et al. (1995b), which give  $B_{\text{IIIaJ+GG395}} = B_{\text{IIaO}} - 0.35(B - V)$  and  $B_{\text{IIaO}} \approx B$ .

Lastly, we find in average the red photographic passbands slightly *bluer* than the Cousins R. This contradicts the traditional correction established — photoelectrically, and then extrapolated to photography — by Couch & Newell (1980), who proposed a response for the combination IIIaF+RG630 *redder* than Cousins R. Note that more recent determinations (Cunow & Wargau 1993) also support the idea that the Couch & Newell equation is inappropriate.

In the end, the photographic magnitudes from each plate were corrected using the equations of Table 3.5.3 to yield magnitudes in a unified system. Given the smallness of the colour coefficients, the resulting degradation in photometric accuracy is negligible. The *rms* residual of the calibration above the completeness limit ranges between 0.07 and 0.17 mag (including the contribution from large scale inhomogeneities). Assuming that the intensity scale is perfectly linearized, the formal uncertainty on the individual plate zero-points would be  $\approx 0.02$  mag. But such an assumption is by far too optimistic with photographic plates. Given the number of bright standard galaxies per plate (between 1 and 3 per magnitude), and the *rms* uncertainty on their magnitudes (about 0.15 mag), we estimate the individual zero-point systematic errors to be  $\lesssim 0.1$  mag in the range  $15 < B_J < 21$ , and  $14 < R_F < 19.5$ . As Figure 3 shows, below these fluxes the photometric errors grow rapidly.

### 3.5.4. Comparison with other photometries

Figure 3 shows the differences between photo and CCD magnitudes for our CCD standard galaxies, as well as the comparison with the photometry of bright galaxies

<sup>3</sup> Although our  $R_F$  is photometrically equivalent to Cousins R within the measurement errors, throughout this paper we denote red *photographic* magnitudes “ $R_F$ ” instead of “R”.

<sup>4</sup> It seems that through the years some confusion has often been made between the IIIaJ+GG385 and IIIaJ+GG395 combinations (see for instance Shanks et al. 1984), and yet these prove to lead to somewhat different (although close) passband definitions.

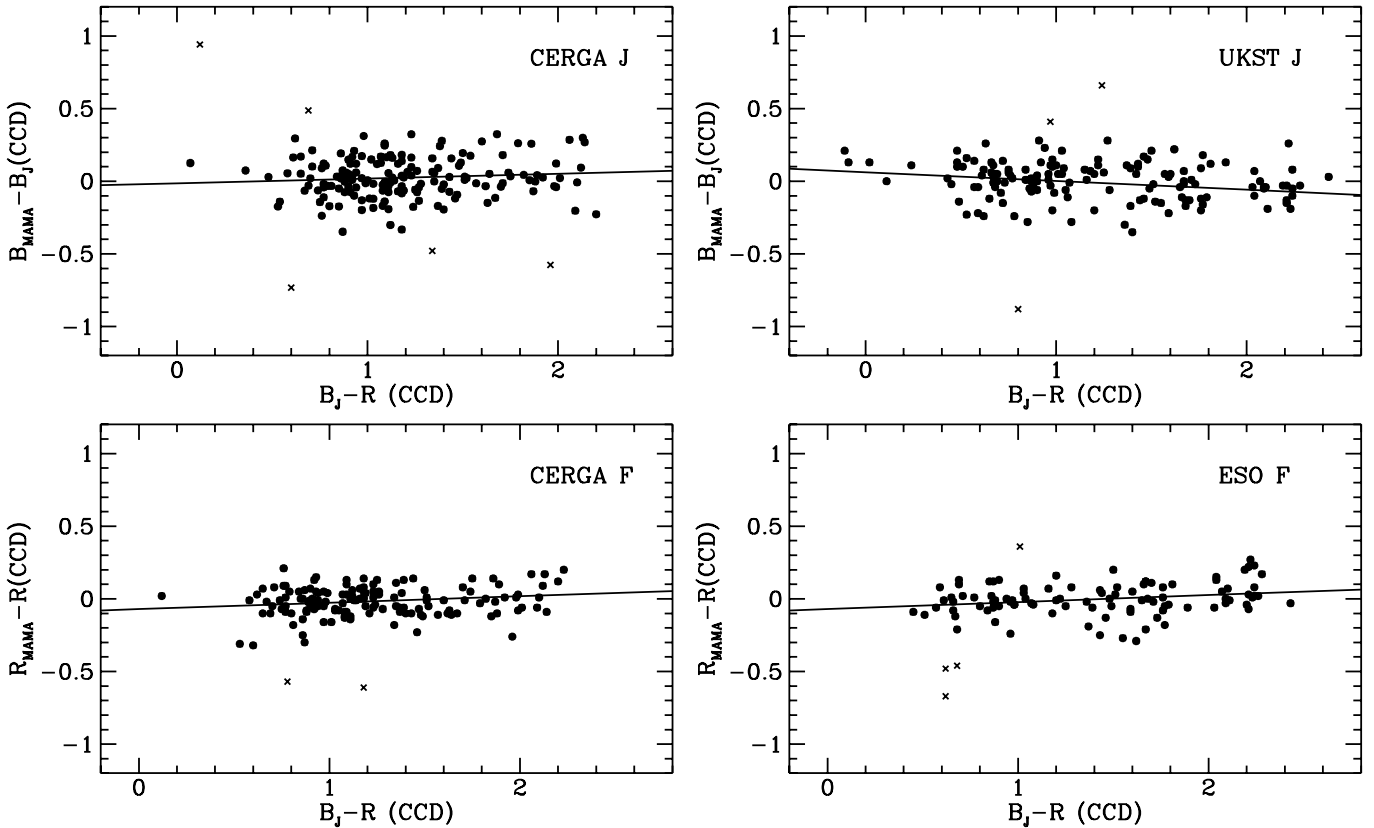


**Fig. 2.** Differences between “pure” (but calibrated) photographic and CCD magnitudes as a function of the  $B_J - R$  colour index for the brightest standards:  $B_J < 20$  (CERGA blue),  $B_J < 21$  (UKST blue),  $R < 18$  (CERGA red) and  $R < 19$  (ESO red). The standards contain about 2/3 of stars and 1/3 of galaxies (which show similar behaviour). A few points (crosses) deviate by more than  $3\sigma$  from the mean relation and have not been taken into account for the chi-square fit (solid line).

**Table 2.** Photographic passbands and their link to standard photometric systems

Plate type	Emulsion+filter	Colour equations	
CERGA “blue”	IIIaJ + GG385	$B_J + (0.033 \pm 0.015) (B_J - R)$	$B - 0.24(B - V)$
UKST “blue”	IIIaJ + GG395	$B_J - (0.060 \pm 0.023) (B_J - R)$	$B - 0.35(B - V)$
CERGA “red”	IIIaF + RG610	$R + (0.044 \pm 0.017) (B_J - R)$	$R + 0.036(B - R)$
ESO “red”	IIIaF + RG630	$R + (0.048 \pm 0.019) (B_J - R)$	$R + 0.039(B - R)$

by several authors. Nine of the galaxies measured by Metcalfe et al. (1995b) are found in our catalog; we find mean differences (MAMA-Metcalfe)  $\Delta B_J = -0.04 \pm 0.08$ , and  $\Delta R_F = -0.07 \pm 0.05$ . Note that 3 of these galaxies also figure among our CCD standards; in both B and R, our magnitudes are in agreement with theirs within 0.02 mag.

Although their photographic photometry does not reach the same accuracy and is more subject to biases than CCD or photoelectric standards, galaxies from the LV catalog (Lauberts & Valentijn 1989) have proven to be in good agreement with the RC3 system (Paturel et al. 1994), and can be used to trace an eventual large systematic trend at bright magnitudes ( $B_J < 16$ ). Over the 4 southern fields we find mean differences (MAMA-LV)  $\Delta B_J = +0.10 \pm 0.05$  and  $\Delta R_F = +0.06 \pm 0.05$ . These

discrepancies might be interpreted as some loss of flux at the bright end ( $B_J \approx 15$ ) of our catalog. However, in the same magnitude range, “CCD galaxies” photometered here or by Metcalfe et al. do not show this offset, which could argue for a small, local zero-point error in the LV magnitudes.

Some bright galaxies ( $B_J \lesssim 15$ ) from the northern plates do also have photoelectric B and V “total” magnitudes in the RC3 catalog. From these we get a mean difference (MAMA-RC3)  $\Delta B_J = +0.15 \pm 0.08$  which reveals the influence of plate saturation at the bright end of our catalog.

Finally, 5 of the galaxies photometered with a CCD by Maddox et al. (1990c) to calibrate the APM survey lie in our field 201 and give an offset (MAMA-APM)

$\Delta B_J = -0.16 \pm 0.14$ . More than this significant offset, the unexpectedly large dispersion of magnitudes — almost 0.3, that is, as much as with the photographic LV sample! — casts some doubt over the reliability of the Maddox et al. calibration set for this plate.

In conclusion, we believe our magnitude scale to be free from any large systematic error, except brightwards of  $B_J \approx 15$ , where fluxes might possibly be underestimated by  $\approx 0.1$  mag.

### 3.6. Merging of catalogs

The “blue” and “red” catalogs were cross-identified in alpha, delta, to yield a unique two-color catalog. Differences in seeing or image quality, as well as imbricated detections (i.e. stars lying on disks of galaxies) were handled through a complex matching algorithm taking into account the shape of detected objects. This procedure leads to a highly reliable catalog, virtually suppressing all false detections like pieces of hair, satellite trails, optical ghosts or spikes around bright stars (these are generally classified as galaxies). One might fear some loss of objects with extreme colours in the final catalog; however the fraction of non-paired detections is almost constant with magnitude, and is about 1% (most of which are spurious), rising to 5% in the last half-magnitude bin imposed by star/galaxy separation.

## 4. Galaxy number counts

### 4.1. Results

The differential number counts are shown for each field in Fig.4. One can notice a great homogeneity over the whole magnitude range between the plates, except for the  $16^h+42^\circ$  field. In fact this field contains no less than 12 Abell clusters, and is part of the Hercules supercluster. One can estimate the variance in number counts at a given depth on a Schmidt plate from the Maddox et al. (1990a) angular two-point correlation function (e.g. Peebles 1980). We find that the projected density of galaxies in the  $16^h+42^\circ$  field exceeds the mean one from the other fields by a factor of  $\gtrsim 4$  times the expected deviation at  $B_J = 15$ , reducing to  $\approx 2$  for  $B_J > 17$ . This field is therefore one of the densest in the sky at the bright end of our catalog, and including it in the total number counts shown in Fig.5 severely changes the slope at  $B_J \lesssim 16$ . For this reason we decided to discard it from the samples for the statistical analysis of number counts, remembering however that we might underestimate in this way the true density of bright galaxies.

### 4.2. Comparison with previous counts

Bright galaxy counts published so far were all conducted on photographic material, in quite similar passbands. This enables us to compare easily our results with previous

work. The transformations we applied are described below.

Many of the existing bright galaxy counts (Shanks et al. 1984, Stevenson et al. 1986, Heydon-Dumbleton et al. 1989) make use of the  $b_j$  passband definition established by Kron (1980), and which transforms to our  $B_J$  through

$$B_J = b_j - 0.05 \quad (4)$$

assuming  $\langle B - V \rangle = 1.0$ . The recent counts of Weir et al. (1995) were done in the Gunn- $g$  passband, for which they give the approximate transformation

$$B_J \approx g - 0.5 \quad (5)$$

to the APM survey magnitude system (Maddox et al. 1990c), which is identical to ours.

Gunn- $r$  observations (Sebok 1986, Picard 1991b, Weir et al. 1995) were transformed to the Cousins R system using

$$R = r + 0.341 \quad (6)$$

from a fit to 16 Landolt standards, giving a standard error of only 0.014 mag (P.Fouqué, private communication). Shanks et al. (1984)  $r_F$  magnitudes were converted with

$$R = r_F - 0.09 \quad (7)$$

inserting  $\langle B - R \rangle = 1.5$  in their equation (5).

As shown on Fig. 6, our counts agree well with those from other studies, especially with the preliminary counts done on POSSII plates (Weir et al. 1995), despite the uncertainties in the conversion from their photometric system to ours. In R, the major discrepancies observed are with Shanks et al. (1984), and the Picard (1991b) northern and southern counts, although our results lie in-between. The Shanks et al. counts are based on only one Schmidt plate, so the fact that they show an offset is perhaps not surprising. As pointed out by Weir et al. (1995), it is yet unclear whether the difference between the Picard counts originates from the presence of very large scale structures, as claimed by Picard (1991a), or are simply caused by unexpected photometric errors in his photometry. We note here that one of our plates lies at about  $20^\circ$  from Picard’s northern field, and that no particular enhancement in galaxy density is seen there.

At their faint end ( $20 < B_J < 21$ ), our blue counts are about 10% lower than those of Weir et al. (1995) and Maddox et al. (1990d); however the raw counts (Fig. 4) do not indicate any obvious drop in completeness at that level. As a matter of fact, two points should be considered here: (1) half of the difference (5%) can be explained by detections that were not matched between the two colours and dropped in the final catalog (although there is no proof that these are real objects), and (2) Weir et al. (1995) showed on simulations that both their counts and

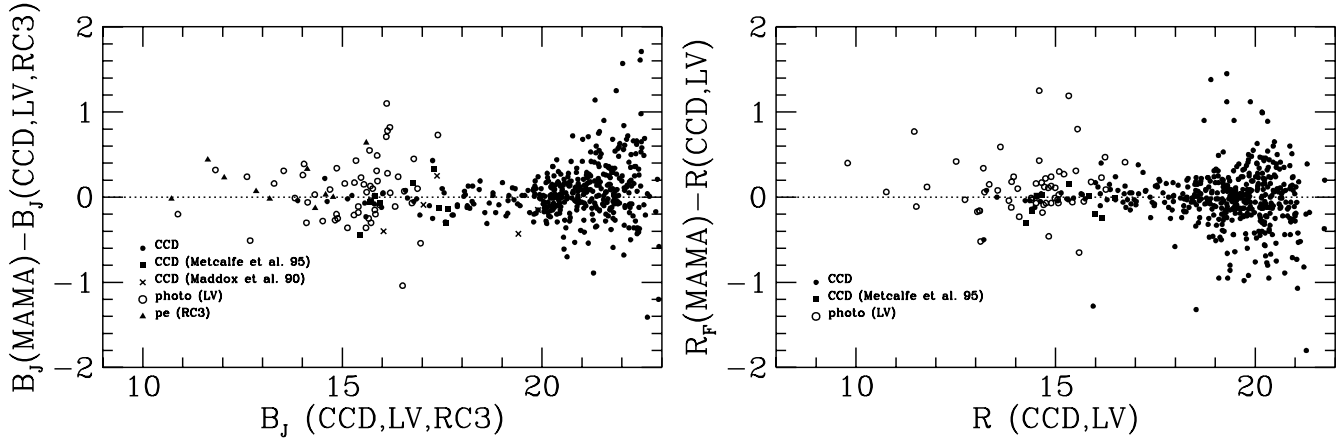


**Fig. 3.** Difference between photographic and CCD magnitude for standard galaxies as a function of CCD magnitude. Photographically unsaturated stars (with  $B_J > 20$  or  $R_F > 18$ ) are added at the faint end. Also displayed are bright galaxies measured by different authors.

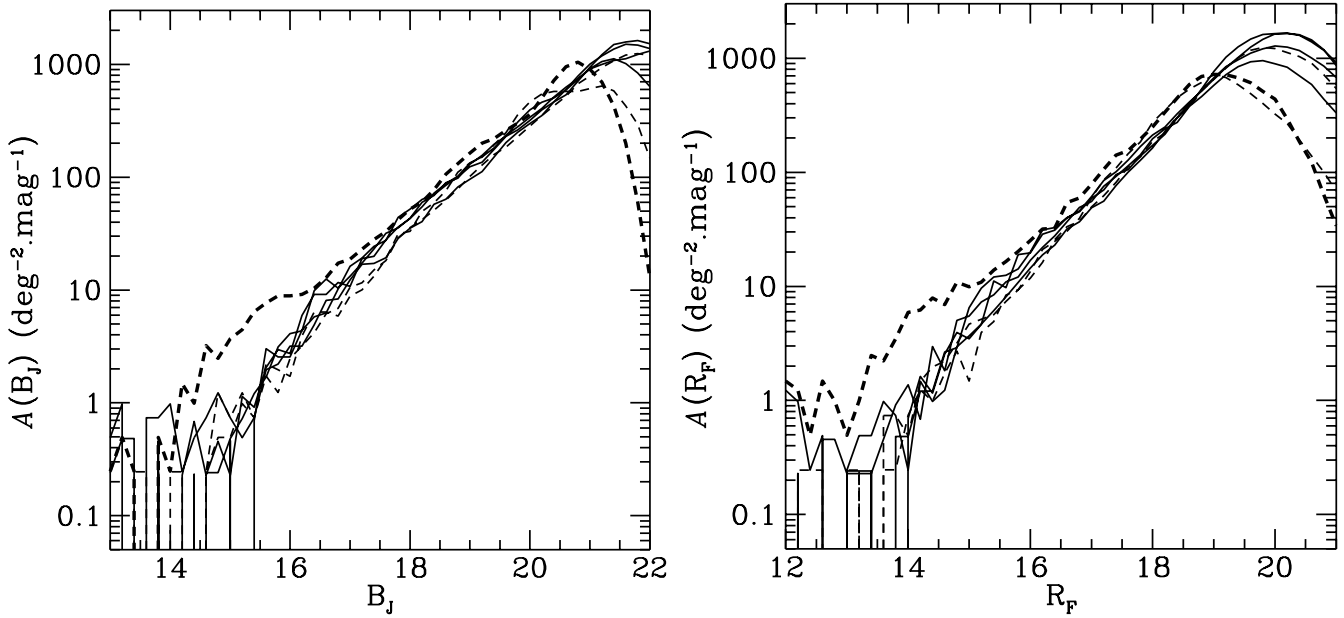


**Fig. 4.** “Raw” differential number counts in  $B_J$  and  $R_F$  for each of the Schmidt fields (continuous line = southern fields; dashed lines = northern fields). Note the excess of galaxies in the northern field  $16^h +42^m$  (thicker lines), especially at bright magnitudes.

those derived by the APM survey might be slightly overestimated (by about 10%) for  $B_J \gtrsim 20$ . Therefore it is likely that this difference at the faint end between our counts and others should not be interpreted as something significant, but only as a consequence of a different data processing. This is confirmed by the recent medium-deep CCD counts by Arnouts et al. 1996, which are in perfect agreement with ours over this magnitude range, in both colours.

But the most interesting discrepancy in this comparison is the one seen with some other galaxy counts at bright magnitudes. At  $B_J = 16.5$  for instance, we count nearly twice as many galaxies as do Maddox et al. (1990d)

or Heydon-Dumbleton et al. (1989). The recent Weir et al. (1995) counts stay however in perfect agreement with ours down to their brightest limit. As the APM survey, because of its statistical weight, is traditionally used to normalize galaxy counts models at bright magnitudes, it is worth investigating further what may be the origin of this difference. Recently, Metcalfe et al. (1995b) have discovered some scale error on the  $17 \lesssim B_J \lesssim 18$  domain in the APM galaxy magnitudes. The APM survey shares four Schmidt fields in common with us, and the corresponding part of the catalog, down to  $B_J = 21$  was kindly provided by J. Loveday for comparison.

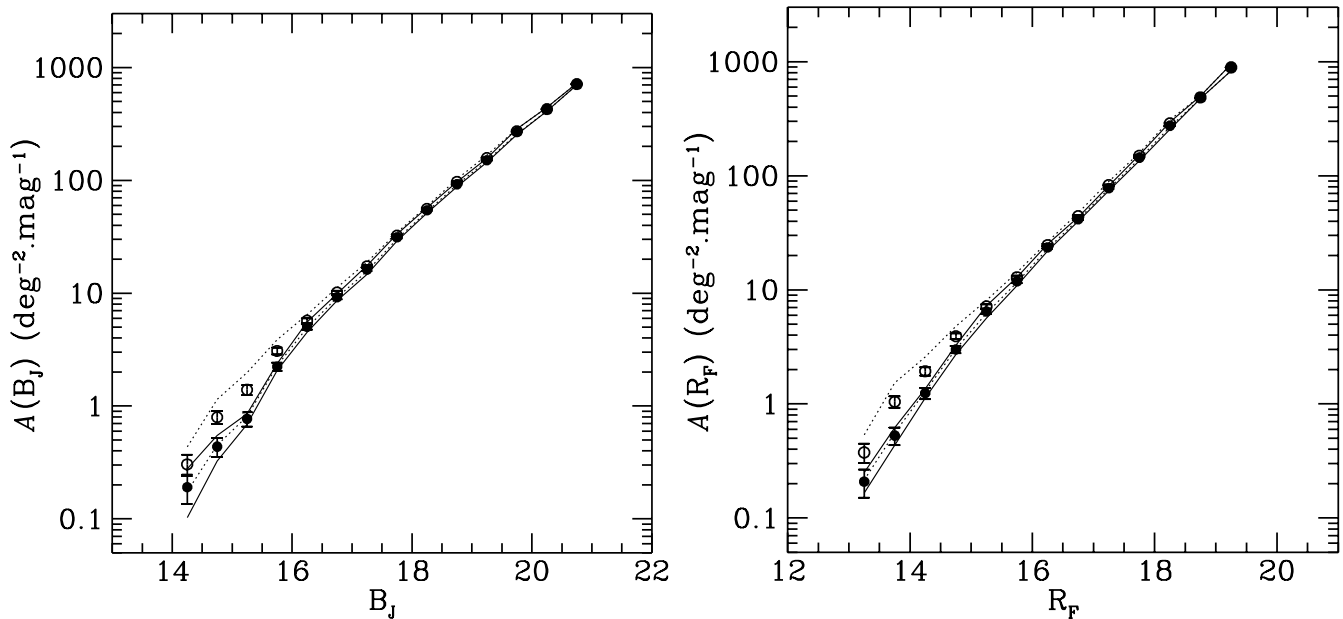


**Fig. 5.** Total differential number counts in  $B_J$  and  $R_F$  in our catalog, including (open circles) or not (filled circles) the  $16^h+42^\circ$  field. Error bars indicate poissonian ( $1\sigma$ ) uncertainties whereas lines bracket the *rms* excursion of the total counts assuming the galaxy density is uncorrelated from plate to plate.

Figure 7 shows the difference between the APM catalog and our magnitudes for each of these four fields<sup>5</sup>. Although both magnitudes are in agreement within  $\approx 0.1$  mag. at the faint end ( $B_J \geq 20$ ), one can immediately notice a systematic difference at brighter magnitudes, reaching 0.3 to 0.5 mag. at  $B_J \approx 16-17$ . To find out whether this was due to our calibration or was intrinsic to the APM data, we cross-identified our list of southern standard galaxies with the APM catalog to produce a plot similar to Fig. 3. Figure 8 shows indeed that there seems to be some problem in the magnitude scale of this APM galaxy sample. The magnitude overestimate starts to rise at  $B_J \approx 19.5$  and increases until  $B_J \approx 17$  where it culminates at about 0.4 mag. Brighter than this point, it is unclear whether it stays at the same level or decreases again, but at  $B_J \approx 15-16$  the offset is still at least about 0.2 mag. Of course these estimates are in principle only valid for the small subsample of the APM catalog considered here, and might not be applicable to the full catalog. But one can see that compensating for this average trend in the magnitude scale would bring the total APM counts in very good agreement with ours.

<sup>5</sup> The version of the APM catalog shown here uses plate-to-plate matching based only on the faintest magnitude bin ( $19.5 < b_j < 20.5$ ). The actual version used for statistical studies, limited to  $b_j > 17$ , uses matching in three magnitude ranges (G. Dalton, private communication). However, a comparison between the two versions for our zone shows an average difference (unmatched–matched) peaking to only  $\approx +0.06$  mag. at  $b_j = 17$ .

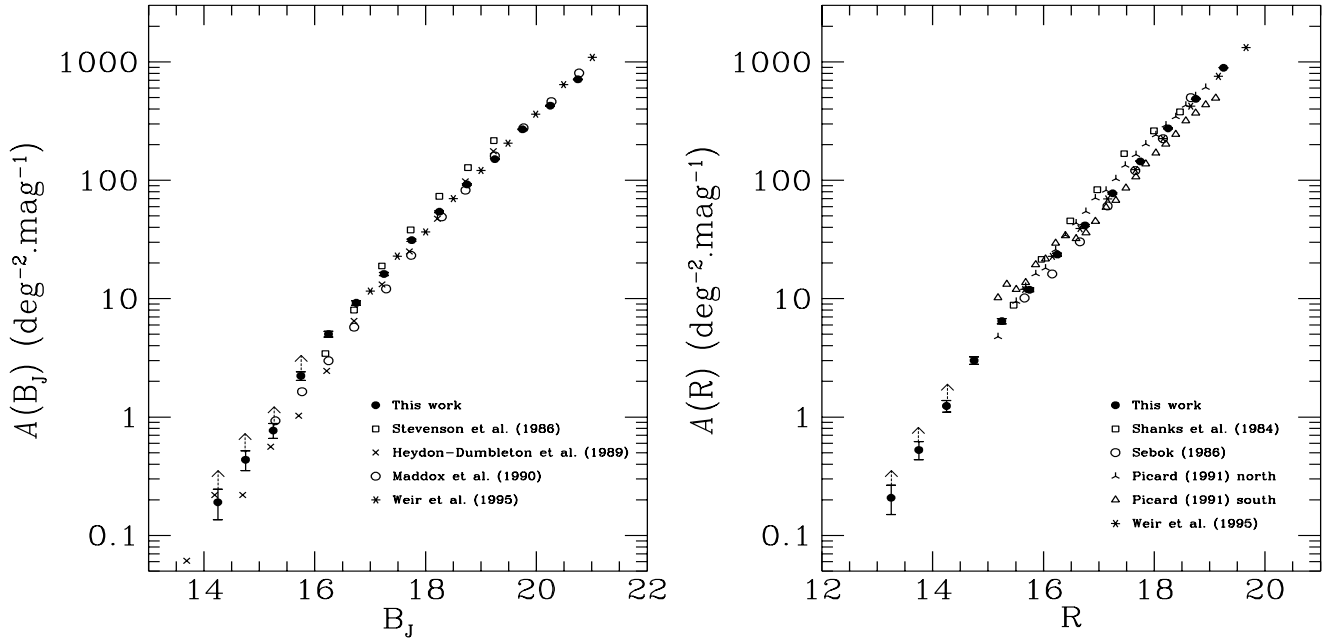
## 5. Comparison with models

### 5.1. Numbers counts and the normalization of the “local” luminosity function

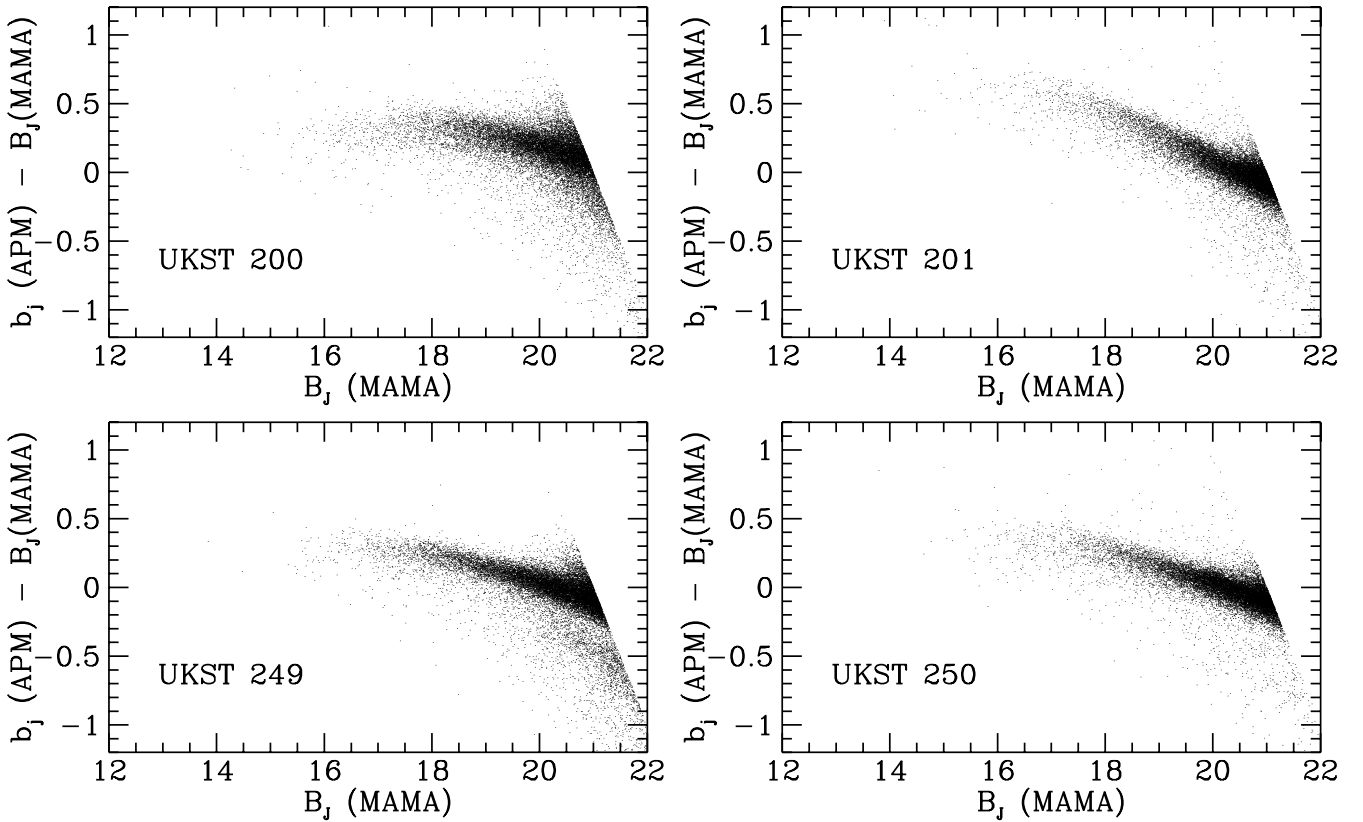
A recurring problem with previous counts has been the normalisation of models at bright magnitudes. Normalizing passively evolving models at  $B_J = 17$  leads to an apparent excess of already 50 to 100% at  $B_J \approx 20-21$ . This apparent phenomenon is hard to reconcile with the redshift distributions to  $B_J \lesssim 23-24$  (Glazebrook et al. 1994, and references therein), which suggest a higher normalisation of the field luminosity function. As our data “push” the bright end of galaxy counts to higher values, we can now test how *local* determinations of the luminosity function are able to match the counts over the domain  $16 \leq B_J \leq 21$ .

We therefore constructed a very simple non-evolving model of galaxy counts, intended to be valid at least to  $B_J \lesssim 20$ . K-corrections were computed by integrating the spectral energy distributions from Pence (1976) through the  $b_j$  and  $r_F$  photographic passbands given by Couch & Newell (1980), which are very close to our blue and red passbands. The morphological mix of galaxy types was taken from Shanks et al. (1984). This model does not include luminosity or number evolution as in deeper count models (e.g. Guiderdoni & Rocca-Volmerange 1990, McLeod & Riecke 1995), but is sufficient for our normalisation purpose. We chose an Einstein-de Sitter universe for simplicity, although at this depth ( $z \lesssim 0.2$ ) the counts





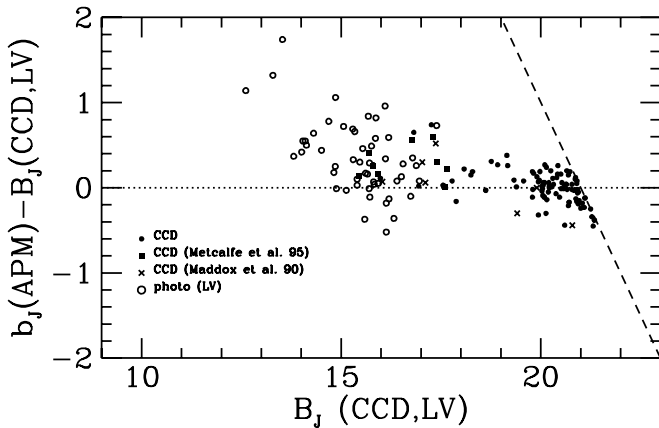
**Fig. 6.** Comparison of published bright galaxy counts converted to our  $B_J, R$  photometric system. Arrows indicate counts underestimated because of incompleteness (3.4).



**Fig. 7.** Comparison of galaxy magnitudes between the APM and our MAMA catalog on four UKST Schmidt plates. The tilted frontier on the right side of the plot is caused by the  $B_J = 21$  limit in the APM subsample.

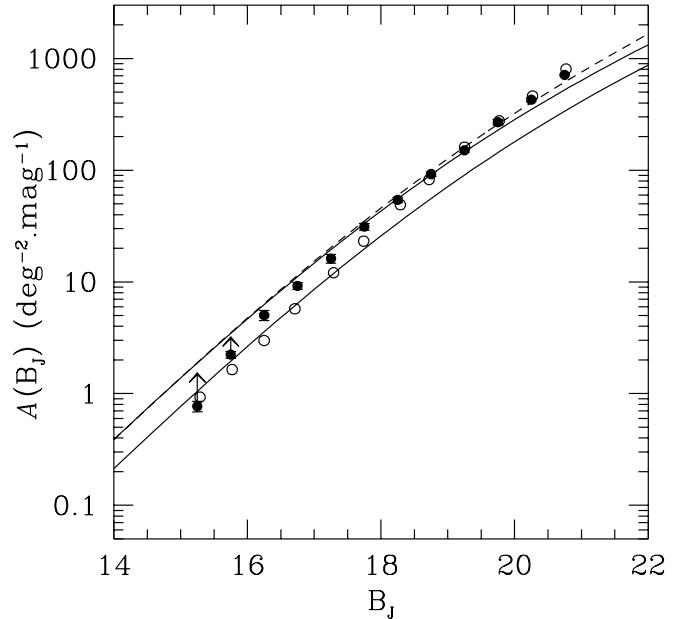
prove to be quite insensitive to (reasonable) cosmological parameters (e.g. Yoshii & Takahara 1988).

Figure 9 shows our data compared to simple galaxy counts models in the blue photographic passband without evolution as described above, using two different luminosity functions (LF). The first one is from Efstathiou et al. (1988, hereafter EEP), from a compilation of results obtained on several redshift surveys, and the second one, more recent, is from Loveday et al. (1992, hereafter LPEM) from a sparse redshift survey of APM galaxies. Schechter parameters are given for both in Table 5.1. A third, colour dependant, LF from Shanks (1990), with the normalisation adopted by Metcalfe et al. (1991) is also shown for comparison. As can be seen, the EEP luminosity function fits the data much better than the one from LPEM, which are however, as expected, in good agreement with the APM counts for  $B_J \leq 17$ . In fact, most of the discrepancy between the two luminosity functions lies in the value of  $M_{B_J}^*$ , with a difference close to 0.4 mag, i.e. about the same one gets when comparing APM magnitudes to those of standard galaxies at  $B_J \approx 17$  (Fig. 8). The best agreement is found with the Shanks LF model. This is not a surprise, as the two other models do not distinguish the luminosity functions of early and late-types, which are indeed quite different; and this shows up when K-corrections become important.



**Fig. 8.** Same as Fig. 3, but with the APM catalog. The dashed line marks the magnitude limit of the APM subsample.

Figure 9 indicates that the normalisation of the Shanks LF adopted by Metcalfe et al. (1991) is in excellent agreement with our own counts, but the latter are still slightly too steep on their bright side compared to any non-evolving model. Can this be interpreted as evolution? One can hardly conclude on the basis of the data presented here, as a 10% misclassification of galaxies added to a 0.1 mag. systematic error in measured fluxes at  $B_J \approx 17$  would be enough to produce this effect.



**Fig. 9.** Comparison of our  $B_J$  galaxy counts (filled circles) and those of the APM survey (open circles) with the simple models described in the text. Errorbars are  $1\sigma$  uncertainties deduced from the field-to-field scatter within each bin (assuming galaxy density is uncorrelated from one plate to another). Arrows indicate points affected by incompleteness. The 3 curves correspond to different luminosity functions used in the no-evolution model: Efstathiou et al. 1988 (upper solid line), Loveday et al. 1992 (lower solid line), and Shanks 1990 as normalized by Metcalfe et al. 1991 (dashed line).

## 5.2. Galaxy colours

Galaxy colour distributions for the total catalog (including the field  $16^h+42^\circ$ ) are presented in Fig. 10. They are in good agreement with the compilation presented by Koo & Kron (1992), if one makes allowance for the passband differences between our system and theirs.

We reemployed the Shanks LF model with no evolution described above to model the observed colour distribution. Rest-frame galaxy colours per Hubble type were taken from Metcalfe et al. (1991) and converted from their CCD photometric passbands to our photographic system with  $(B_J - R_F) = 0.91(B - R)_{\text{CCD}}$ . Ingredients of the LF are gathered in Table 5.2. Photometric errors were included in the model, adopting an error distribution with magnitude determined in the overlap between catalogs (see Bertin 1996). Photometric errors do not only smear out details in the observed colour distribution, they also distort the wings of the distribution for the dimmest objects (that is, when the error strongly evolves with colour). As our red plates are here significantly less sensitive than the blue ones, the two lower graphs in Fig. 10 exhibit a shallower tail on their blue side than on their red side.

**Table 3.** Global Schechter parameters of local luminosity functions ( $H_0 = 100\text{km.s}^{-1}\text{Mpc}^{-1}$ )

	$\alpha$	$M_{B_J}^*$	$\phi^*$ ( $\text{Mpc}^{-3}$ )
Efstathiou et al. (1988)	$-1.07 \pm 0.05$	$-19.97^a \pm 0.10$	$(1.56 \pm 0.34) \times 10^{-2}$
Loveday et al. (1992)	$-0.97 \pm 0.15$	$-19.50 \pm 0.13$	$(1.40 \pm 0.17) \times 10^{-2}$

<sup>a</sup> Converted from  $B_T$  using Eq. (4.1d) from Efstathiou et al.

Observed and predicted distributions prove to be in very good agreement, except in the brightest subsample, where we expect some problems with the saturation and the robustness of star/galaxy separation. One can notice a small ( $\approx 0.1$  mag) systematic colour offset between the two, which might be imputed to uncertainties in our photometric modelling. But no obvious evolution of colour with magnitude is detected, within the uncertainties, up to  $B_J \lesssim 21$ .

**Table 4.** Luminosity function parameters for the colour distribution model ( $H_0 = 100\text{km.s}^{-1}\text{Mpc}^{-1}$ )

	$\alpha$	$M_{B_I}^*$	$\phi^*$ ( $\text{Mpc}^{-3}$ )	$\langle B_J - R_F \rangle$
E/S0	-0.7	-19.6	$1.2 \times 10^{-3}$	1.32
Sab	-0.7	-19.6	$3.9 \times 10^{-3}$	1.15
Sbc	-1.1	-19.9	$6.9 \times 10^{-3}$	0.96
Scd	-1.5	-20.1	$2.7 \times 10^{-3}$	0.70
Sdm	-1.5	-20.1	$1.7 \times 10^{-3}$	0.62

## 6. Discussion

### 6.1. A magnitude scale error in the APM data?

The apparent rapid increase in number counts of galaxies in the magnitude range  $16 \lesssim B_J \lesssim 19$  reported by Maddox et al. (1990d) is thus absent from our counts (or those of Weir et al. 1995), although our slope of  $dN/dm$  is still slightly higher than what predict no-evolution models at  $B_J \lesssim 17$ . As the comparison with the APM data seems to indicate, this might be essentially due to a difference in magnitude scale of  $\approx 0.1$ - $0.2$  mag./magnitude. Serious suspicions about systematic residual errors in the APM magnitudes at  $B_J \approx 17 - 18$  have recently been raised by Metcalfe et al. (1995a). If our data are correct, they support and even strengthen this hypothesis. Other arguments also consolidate this idea.

First, our data (Fig. 10), as well as previous ones (see Koo & Kron 1992), do not present evidence for evolution of galaxy colours over the range  $17 \leq B_J \leq 21$ . and rule out strong luminosity evolution scenarios in the visible (McLeod & Rieke 1995) for bright field galaxies, out to  $z \approx 0.2$ .

One might also think of a “giant local void” that would affect the bright end of the counts. Although there are indications of large fluctuations in projected galaxy density at the level of a Schmidt field (Fig. 4, Picard 1991b)

for  $B_J \lesssim 17$ , or over the full sky for  $B_J \lesssim 12$  (Paturel et al. 1994), the analysis of a large spectroscopic subsample (Loveday et al. 1992) seems to exclude this possibility in the APM survey.

Statistics of CCD calibrations (Maddox et al. 1990d, Loveday et al. 1992) done on the APM magnitudes do not reveal any important trend like the one in Fig. 7 and 8. This is quite puzzling, and one might wonder if the effects seen here are not purely local and compensated somewhere else in the APM survey. If this were true, correlated systematic magnitude errors of  $\approx 0.4$  mag., over such large areas (100 sq. deg. in our case) would artificially boost the two-point correlation function on scales  $\gtrsim 5^\circ$  in  $B_J \lesssim 18$  magnitude bins. This does not appear prominently in Fig. 2 of Maddox et al. (1990a). Another clue is that the trend found by Metcalfe et al. (1995a) concerns the whole area of the APM catalog, and therefore supports the hypothesis of a global magnitude scale error (which does not exclude large scale variations of the zero-point).

### 6.2. Uncertainties in the “local” field luminosity function

To partially bypass uncertainties in the optimum Schechter parameters of the local luminosity function for field galaxies, count models are generally “renormalized” by adjusting the Schechter density parameter  $\phi^*$  to counts at some bright magnitude. However, the  $M^*$  parameter itself is directly affected by any systematic error in the magnitude zero-point of a redshift survey. Such errors are known to exist at bright magnitudes in photographic catalogs (Metcalfe et al. 1995b, Yasuda et al. 1995) on which are essentially based all the determinations of the local field luminosity function. In fact, decreasing the  $M^*$  found by LPEM by about 0.4 mag., like our photometric comparison with the APM catalog suggests, brings their luminosity function in good agreement with both the one from EEP and our bright galaxy counts (Fig. 9), without having to increase  $\phi^*$ . One should also note that such a “bright” normalisation in  $M^*$  of the luminosity function removes any significant luminosity evolution<sup>6</sup> of luminous galaxies in the blue band to  $z \approx 0.2$  (Lonsdale & Chokshi 1993).

<sup>6</sup> The related case of evolution in the far-infrared as seen by IRAS will be addressed in a forthcoming paper (Bertin et al., in preparation).

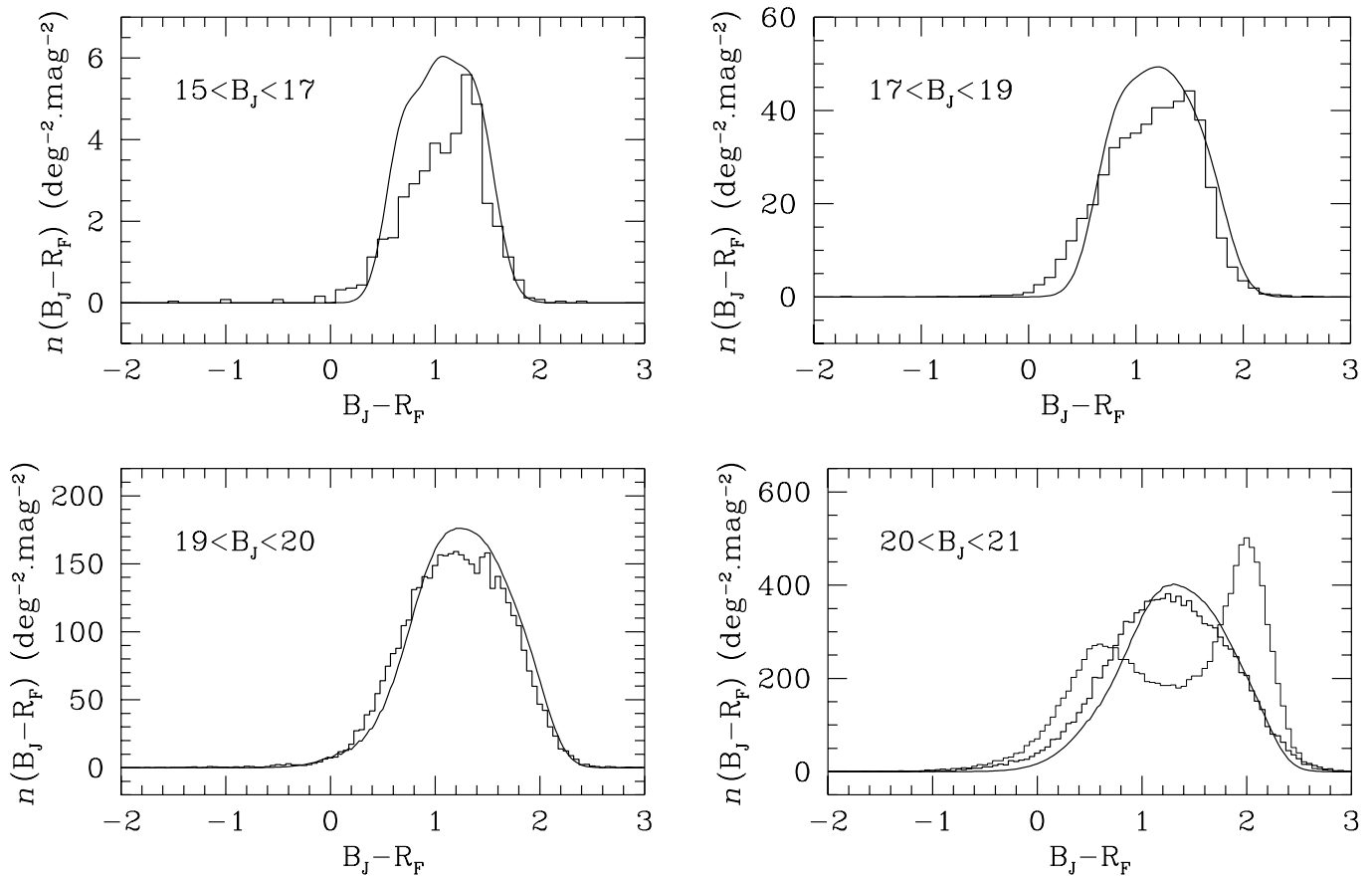


**Fig. 10.** Colour histograms of galaxies compared with the no-evolution model (curves) described in the text, in 4 magnitude intervals. The colour distribution of stars (thin histogram) is plotted for comparison in the faintest subsample.

## 7. Summary and Conclusions

We have presented a new photometric survey of bright galaxies with  $15 < B_J < 21$  and  $14 < R_F < 19.5$ . Comparison with our own CCD galaxy standards, as well as others from the literature, allowed us to estimate systematic errors in the photometry to be  $\lesssim 0.1$  mag over the whole magnitude range of the survey. Our data reveal no evidence of strong galaxy evolution as had been reported by Maddox et al. (1990d) with the APM survey, although the slope of our number counts is still somewhat higher than what is predicted by no-evolution models brightward  $B_J \approx 17$ . A comparison with the APM data and other arguments suggest that the APM catalog is affected by a large magnitude scale error, underestimating by about 0.4 mag the flux of galaxies with  $B_J \lesssim 17$ . This would then justify the choice of a “high” normalization of the field luminosity function (concerning  $M^*$  as well as  $\phi^*$ ) already used by several authors to improve the fit of models at  $B_J > 19$  (e.g. Metcalfe et al. 1991, 1995a, Glazebrook et al. 1994).

But, given the difficulties inherent to photographic photometry, it would be good to confirm our analysis with linear detectors in order to conclude definitively. Forth-

coming digital large scale surveys like the SDSS (e.g. Kent 1994) should provide this possibility.

*Acknowledgements.* We thank the team from CERGA, especially D.Albanese and C.Pollas for providing the northern Schmidt plates; the MAMA team, especially R. Chesnel and O. Moreau for their high-quality scans; P.Fouqué for enlightening discussions about the local universe and galaxy photometric systems; J. Loveday and G. Dalton for providing the APM comparison subsamples; and our referee for useful suggestions.

## References

- Arnouts S., de Lapparent V., Mathez G., Mazure A., Mellier Y., Bertin E., Kruszewski A., 1996, accepted for publication in A&AS
- Berger J., Fringant A.M., Guibert J., Moreau O., Cordoni J.P., 1991, A&AS 87, 389
- Bertin E., 1994, Ap&SS 217, 49
- Bertin E., Arnouts S., 1996, A&AS, in press (BA96)
- Bertin E., Dennefeld M., Moshir M., in preparation
- Bertin E., 1996, *Thèse de Doctorat*, Université Paris VI
- Blair M., Gilmore G., 1982, PASP 94, 742
- Bruzual A.G., Charlot S., 1993, ApJ 405, 538
- Couch W.J., Newell E.B., 1980, PASP 92, 746
- Cunow B., Wargau W.F., 1993, A&AS 102,331

- Glazebrook K., Ellis R., Colless M., Broadhurst T., Allington-Smith J., Tanvir N., 1994, MNRAS 273, 157
- Efstathiou G., Ellis R.S., Peterson B.A., 1988, MNRAS 232, 431 (EEP)
- Guiderdoni B., Rocca-Volmerange B., 1990, A&A 227, 362
- Heydon-Dumbleton N.H., Collins C.A., McGillivray H.T., 1989, MNRAS 238, 379
- Hubble E., 1926, ApJ 64, 321
- Infante L., 1987, A&A 183, 177
- Irwin M.J., 1985, MNRAS 214, 575
- Irwin M.J., Hall P., 1983, in Proc. Workshop Astronomical Measuring Machines (eds Stobie R.S. & McInnes B.), ROE, Edinburgh, 111
- Jarvis J.F., Tyson J.A., 1981, AJ 86, 476
- Jones L.R., Fong R., Shanks T., Ellis R.S., Peterson B.A., 1991, MNRAS 249, 481
- Kent S.M., 1994, in Science with Astronomical Near-Infrared Surveys (eds N. Epchtein, A. Omont, B. Burton, P. Persi), Kluwer, Dordrecht, 27
- Koo D.C., Kron R.G., 1992, ARA&A 30, 613
- Kron R.G., 1980, ApJS 43, 305
- Lauberts A. & Valentijn E.A. 1989, The Surface Photometry Catalogue of the ESO-Uppsala Galaxies, European Southern Observatory.
- Lonsdale C.J., Chokshi A., 1993, AJ 105, 1333
- Loveday J., Peterson B.A., Efstathiou G., Maddox S.J., ApJ 390, 338 (LPEM)
- Maddox S.J., Efstathiou G., Sutherland W.J., Loveday J., 1990a, MNRAS 242, 43p
- Maddox S.J., Sutherland W.J., Efstathiou G., Loveday J., 1990b, MNRAS 243, 692
- Maddox S.J., Efstathiou G., Sutherland W.J., 1990c, MNRAS 246, 433
- Maddox S.J., Sutherland W.J., Efstathiou G., Loveday J., Peterson B.A., 1990d, MNRAS 247, 1p
- Majewski S.R., 1992, ApJS 78,87
- McLeod B.A., Rieke M.J., 1995, ApJ 254, 611
- Metcalfe N., Shanks T., Fong R., Jones L.R., 1991, MNRAS 249, 498
- Metcalfe N., Shanks T., Fong R., Roche N., 1995a, MNRAS 273, 257
- Metcalfe N., Fong R., Shanks T., 1995b, MNRAS 274, 769
- Moreau O., 1992, *Thèse de Doctorat*, Université Paris VII
- Paturol G., Bottinelli L., Gouguenheim L., 1994, A&A 286, 768
- Paturol G., Bottinelli L., Di Nella H., Fouqué P., Gouguenheim L., Teerkorpi P., 1994, A&A 289, 711
- Peebles P.J.E, 1980, The Large scale Structure of the Universe, Princeton University Press, Princeton
- Pence W., 1976, ApJ 203, 39
- Picard A., 1991a, ApJL 386, L7
- Picard A., 1991b, AJ 102, 445
- Reid N., Gilmore G., 1982, MNRAS 201, 73
- Röser S., Bastian U., 1991, PPM Star Catalogue, Astronomisches Rechen Institut Heidelberg (Germany)
- Schechter P., 1976, ApJ 203, 297
- Sebok W.L., 1986, ApJS 62, 301
- Seitter W.C, 1988, in Large-Scale Structures in the Universe - Observational and Analytical Methods (eds W.C. Seitter et al.), Lecture Notes in Physics 310, Springer, Berlin, 9
- Serrat-Ricart M., Trapero J., Beckman J.E., 1995, AJ 109, 312
- Shanks T., Stevenson P.R.F., Fong R., MacGillivray H.T., 1984, MNRAS 206, 767
- Shanks T., 1990, in Galactic and Extragalactic Background Radiation (ed Mattilla K.), Reidel, Dordrecht, 269
- Smail I., Hogg D.W., Yan L., Cohen J.G., 1995, Accepted for publication in ApJ Letters
- Stevenson P.R.F., Shanks T., Fong R., 1986, in Spectral Evolution of Galaxies (eds Chiosi C. & Renzini A.), Reidel, Dordrecht, 439
- Sutherland W.J., Maddox S.J., Saunders W., McMahon R.G., Loveday J., 1991, MNRAS 248, 483
- Tyson J.A., 1988, AJ 96, 1
- de Vaucouleurs G., de Vaucouleurs A., Corwin H.G., Buta R.J., Paturol G., Fouqué P., 1991, Third Reference Catalogue of Bright Galaxies, Springer, New York
- Weir N., Djorgovski S., Fayyad U.M., 1995, AJ 110, 1
- Yasuda N., Okamura S., Fukugita M., 1995, ApJS 96, 359
- Yoshii Y., Takahara F., 1988, ApJ 326,1